nature biotechnology

ARTICLES

https://doi.org/10.1038/s41587-022-01339-6

Spatiotemporal multiplexed immunofluorescence imaging of living cells and tissues with bioorthogonal cycling of fluorescent probes

Jina Ko[1], Martin Wilkovitsch[2], Juhyun Oh[1], Rainer H. Kohler[1], Evangelia Bolli[1,3], Mikael J. Pittet[1,3,4,5], Claudio Vinegoni[1], David B. Sykes[6,7], Hannes Mikula[2], Ralph Weissleder[1,8] ✉ and Jonathan C. T. Carlson[1,7] ✉

Cells in complex organisms undergo frequent functional changes, but few methods allow comprehensive longitudinal profiling of living cells. Here we introduce scission-accelerated fluorophore exchange (SAFE), a method for multiplexed temporospatial imaging of living cells with immunofluorescence. SAFE uses a rapid bioorthogonal click chemistry to remove immunofluorescent signals from the surface of labeled cells, cycling the nanomolar-concentration reagents in seconds and enabling multiple rounds of staining of the same samples. It is non-toxic and functional in both dispersed cells and intact living tissues. We demonstrate multiparameter ($n \geq 14$), non-disruptive imaging of murine peripheral blood mononuclear and bone marrow cells to profile cellular differentiation. We also show longitudinal multiplexed imaging of bone marrow progenitor cells as they develop into neutrophils over 6 days and real-time multiplexed cycling of living mouse hepatic tissues. We anticipate that SAFE will find broad utility for investigating physiologic dynamics in living systems.

Temporal processes are often studied in living cells and organisms by introducing fluorescent proteins coupled to a promoter[1], protein[2] or biological compartment[3] of interest, making otherwise invisible physiologic events observable by fluorescence microscopy. This strategy has been intensely successful in cell biology[4]. However, the approach is not without shortcomings, including (1) the time required for creation and validation of cell lines; (2) the limited number of concurrent targets that can be visualized; and (3) the practical impossibility of using fluoroprotein labeling to analyze intact ensembles of primary cells, especially in complex contexts, such as development, differentiation or immune function. Optimized monoclonal antibodies make immunofluorescence techniques a feasible alternative to study genetically unmodified cells both in vitro[5] and in vivo[6,7] but only for a handful (that is, 1–4) of simultaneous targets. In aggregate, these liabilities sharply restrict the dimensionality of our view into living systems.

An array of analytical technologies, such as cellularly resolved sequencing[8–11], multiplexed immunostaining[12–16], mass/imaging cytometry[17–20] and synergistic combinations thereof[21,22], can now achieve detailed snapshots of biomarker abundance, producing fine-grained but static profiles. Nevertheless, the techniques are thus far incompatible with making measurements in living cells or tissues, due to inherently lethal physicochemical processing during the analytical workflow or single-cell detection mechanisms, as in flow cytometry[23], that cannot observe cells in situ (that is, within the context of their growth environment). Of the above tools, only the methods that rely on iterative immunostaining are potentially non-destructive, as the key step of antibody–antigen recognition is intrinsically biocompatible. The competing priorities, however, of fast/complete cycling and live-cell gentleness/non-toxicity require chemical conditions that have remained orders of magnitude apart (Supplementary Fig. 1). Transient binding of antibodies (as in uPAINT[24]) or nucleic acid probes (as in DNA-PAINT[25]) have been exploited for super-resolution imaging and could, in principle, be applied to multiplexed analyses of live cells. However, to date, the extended acquisition times and operational complexity of stochastic single-molecule imaging have been limited to fixed samples. As a result, highly multiplexed temporospatial profiling of living cells has been virtually impossible.

Lacking such methods, certain biological processes have remained challenging to investigate, for example: (1) the role of intercellular communication during differentiation[5,26] or immunotherapy[27,28]; (2) functional exploration of novel cellular phenotypes, particularly in the space of immunology[29–31]; and (3) tracing of cellular lineages, for example in hematopoietic development[32]. Experimental techniques to directly observe these events offer the possibility of interrogating biological interactions, developmental transformations and the downstream responses. Further development of such dynamic model systems has thus far been hindered by the inability to efficiently visualize both biomolecular complexity and (multi)cellular dynamics in real time.

We envisioned that new bioorthogonal chemistries could achieve the capabilities needed for longitudinal multiplexed profiling of extracellular markers in live cells (Fig. 1). Here we describe the development and application of the scission-accelerated fluorophore exchange (SAFE) method, which leverages cooperative bioorthogonal mechanisms to first quench and then completely remove fluorescent signal from antibody-labeled cells. With a scaffold built

[1]Center for Systems Biology, Massachusetts General Hospital, Boston, MA, USA. [2]Institute of Applied Synthetic Chemistry, TU Wien, Vienna, Austria. [3]Department of Pathology and Immunology, University of Geneva, Geneva, Switzerland. [4]Ludwig Institute for Cancer Research, Lausanne Branch, Zurich, Switzerland. [5]AGORA Cancer Center, Lausanne, Switzerland. [6]Center for Regenerative Medicine, Massachusetts General Hospital, Boston, MA, USA. [7]Department of Medicine, Massachusetts General Hospital, Harvard Medical School, Boston, MA, USA. [8]Department of Systems Biology, Harvard Medical School, Boston, MA, USA. ✉e-mail: rweissleder@mgh.harvard.edu; carlson.jonathan@mgh.harvard.edu

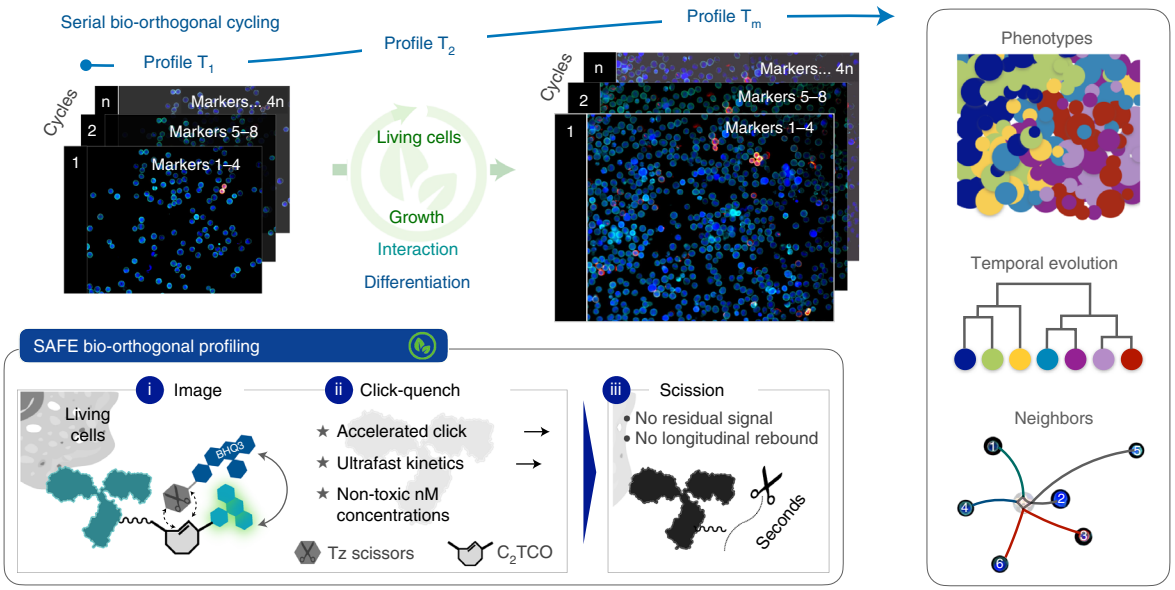

Fig. 1 | Multiplexed temporospatial profiling in living cells. Serial bioorthogonal cycling can reveal complex cellular dynamics in living cells, enabling phenotypic characterization and longitudinal tracking of temporal evolution and/or neighbor–neighbor interactions. Inset: the design of SAFE combines an accelerated click-quenching reaction with rapid fluorophore scission to gently, efficiently and irreversibly erase fluorophores from the surface of immunostained living cells in seconds.

around a cleavable C_2-symmetric *trans*-cyclooctene (C_2TCO), SAFE exploits non-covalent quencher–fluorophore interactions to accelerate already rapid tetrazine (Tz)–TCO click reactions, reaching >99% scission in seconds. Critically, this makes bioorthogonal cycling feasible at non-toxic nanomolar concentrations, which was not possible with previous methods[33], all while achieving the high signal to background needed for serial profiling. We first quantify the accelerated chemical kinetics in analytical fluorescence assays and verify the scission performance in the biological context by time-resolved imaging. We then proceed to validate the accuracy and non-toxicity of 14-color imaging of living mouse peripheral blood mononuclear cells (PBMCs), perform multiplexed imaging experiments in living murine hepatic tissue and visualize myeloid subsets in multicolor staining of living murine bone marrow. Finally, we demonstrate the ability of serial bioorthogonal cycling to track the differentiation of immortalized hematopoietic progenitor cells into neutrophils in longitudinal profiling of the same cells over 6 days.

Results

Bioorthogonal cooperativity accelerates scission. For all but the most reactive molecules, chemical processes that reach completion in the timeframe of seconds to minutes require concentrations in the high micromolar to millimolar range. Although this is no obstacle for in vitro organic synthesis, it poses challenges for bioorthogonal methods: (1) these same concentration ranges correspond to the level at which many organic compounds become non-specifically cytotoxic, barring use in living cells; and (2) reagents with the highest degree of reactivity are typically metastable and/or vulnerable to rapid degradation, limiting their performance in the biological environment[34]. To circumvent these issues, the design of SAFE exploits a cooperative interaction between the fluorescence quencher BHQ3 and Alexa Fluor dyes for rapid on/off scission of fluorophore–C_2TCO-labeled antibodies (Fig. 2a) at low, non-toxic reagent concentrations. Notably, the BHQ3–dye interaction is expected to accelerate the Tz–TCO click reaction; in this initial stage, ligation yields immediate quenching (>95%) of the dye fluorescence[33]. In turn, quantitative scission is driven by a functionalized tetrazine equipped with an intramolecular proton donor (NH_3^+ at physiologic pH) that serves to accelerate tautomerization, functioning as a 'Tz-scissors'[35–37]. This click-to-cut scission reaction then releases the quenched fluorophores from antibodies, removing residual signal: (1) optimizing signal to background and (2) eliminating the downstream risk of rebounding signal from the quenched dye.

We, therefore, synthesized N-Boc-protected tetrazine (**1**) and extended it with a PEG_4 amino acid linker, followed by coupling with BHQ3-amine and deprotection (Fig. 2b). The reaction of BHQ3-N-Tz (**2**) and an AF647–C_2TCO (SAFE647)-labeled antibody was followed by monitoring fluorescence intensity versus time. At an optimized concentration of **2**, the reaction process could be kinetically segregated into its two component phases, resolving the quenching of the click ligation from the subsequent scission reaction. Non-linear fitting of the biphasic fluorescence time course yielded a rate constant of $0.143 \pm 0.005\,s^{-1}$ ($t_{1/2} = 5\,s$) for the scission of the C_2TCO linker. For the click ligation itself, we measured an effective second-order rate constant of $1.18 \pm 0.05 \times 10^6\,M^{-1}s^{-1}$ (Supplementary Fig. 2), more than 2,900-fold faster than the reaction of the parent Tz (**3**) with C_2TCO[37]. C_2TCO itself is stable (>97% intact at $t = 48\,h$ in full cell growth media) and not very reactive until accelerated by the cooperative SAFE effect, resulting in stable click reagents but also very fast kinetics. The cooperative acceleration shifts the kinetic regime from hours to seconds (Fig. 2c). To validate the solution kinetics in a biological context, we stained fixed A431 cells with a SAFE647-labeled anti-EGFR antibody and collected serial images before and after the addition of BHQ3-N-Tz (500 nM; Fig. 2d). The quenching/cleavage reaction on the surface of the cells was both rapid ($t_{1/2} = 1.9\,s$) and complete, with a 99.7% reduction in signal intensity after 40 s (~8 scission half-lives). Control experiments confirmed that the fluorescence dynamics are not driven by photobleaching (Supplementary Fig. 3). These kinetics integrate both steps of signal removal at the extracellular surface, confirming the magnitude of the acceleration and the high dynamic range of signal elimination, critical to minimizing background accumulation and maintaining image quality across multi-cycle staining (Supplementary Fig. 1).

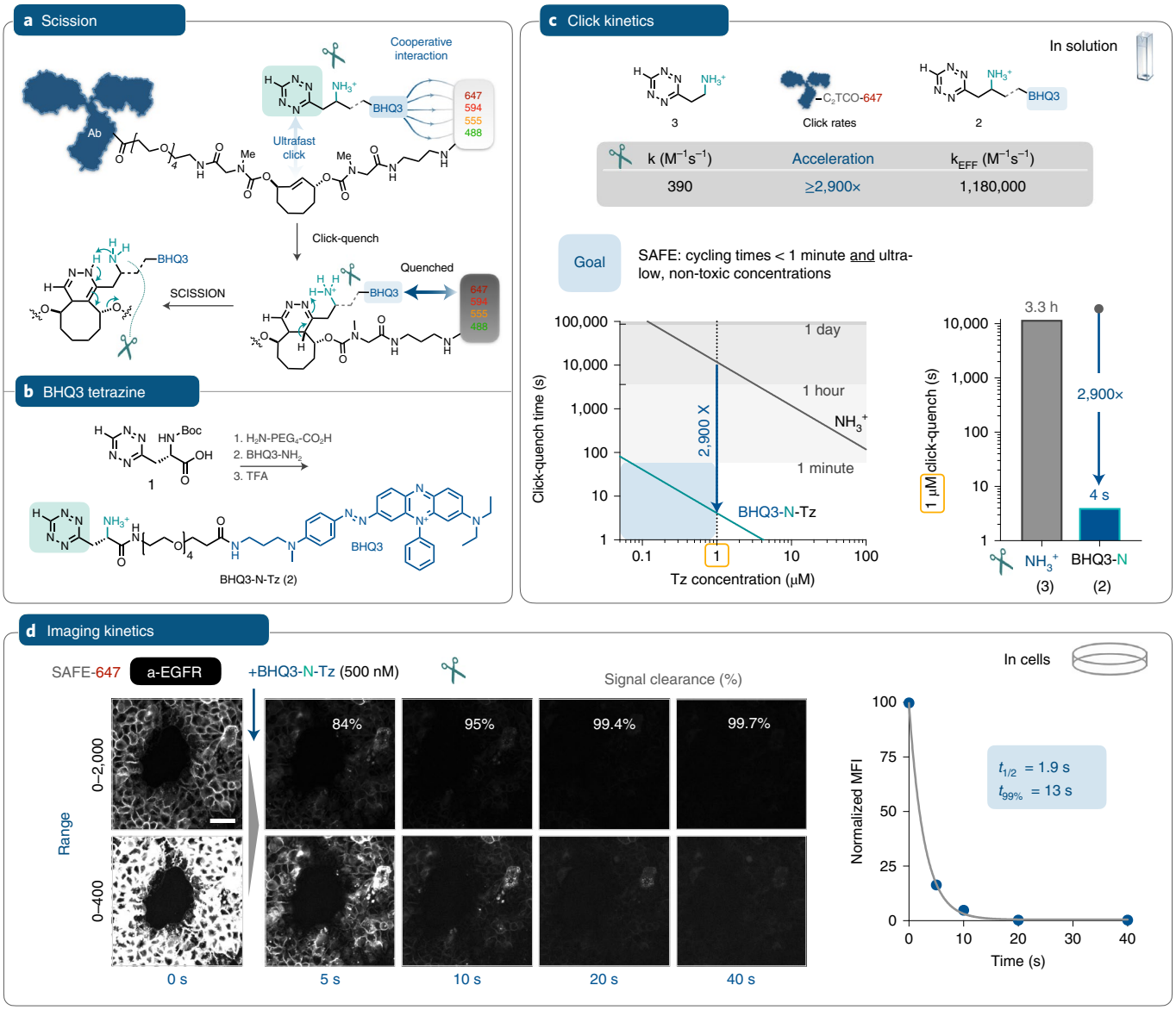

Fig. 2 | Mechanisms, synthesis and kinetics. a, Antibodies labeled with C_2TCO-linked dyes are rendered non-fluorescent in a concerted two-step sequence: non-covalent interactions between BHQ3 and the fluorophore can accelerate the Tz–TCO click reaction[33], leading to immediate quenching upon ligation; in turn, the functionalized 'Tz-scissors' drives instantaneous tautomerization and scission of the dye. The design of C_2TCO itself ensures that the cleavage reaction proceeds irrespective of the Tz–TCO click orientation. **b**, Starting from the Boc-protected Tz (**1**), a hydrophilic PEG linker and BHQ3 are conjugated and then deprotected to yield BHQ3-N-Tz (**2**). **c**, Quantification of reaction kinetics for the click reaction of (**2**) with an AF647–C_2TCO-labeled antibody in solution revealed an effective rate constant of >10^6, a marked ~3,000-fold acceleration relative to the parent aminoethyl-functionalized Tz (**3**)[37]. This acceleration shifts the concentration–time relationship into the needed range for efficient cycling at ≤1 μM reagent concentrations. **d**, To validate the accelerated kinetics in the cellular context, we collected time lapse images of A431 cells stained with a SAFE647-anti-EGFR antibody and then treated with BHQ3-N-Tz (**2**). Images rendered at two window levels capture the rapid ($t_{1/2}$ = 1.9 s, one-phase decay) and quantitative clearance of the fluorophore signal, reaching 99.7% removal within 40 s, concordant with the in vitro assay result. See Supplementary Fig. 3 for analytical details. Normalized mean fluorescence intensity (MFI) is plotted as mean ± s.d.; error bars are smaller than the symbol size. Scale bar, 50 μm.

SAFE allows cycling in live cells. We performed an initial short-term cycling experiment on live A549 cells stained with Hoechst and a SAFE647-conjugated anti-N-cadherin antibody. The N-cadherin signal was promptly eliminated with BHQ3-N-Tz (1 μM, 1 minute; Fig. 3a). A fraction of cells visually confirmed their live status by undergoing mitosis during the imaging process: in the example shown (Fig. 3a, inset), a cell is captured in metaphase before quenching and in early anaphase after quenching, 17 minutes of elapsed time later. For a longer-term assessment, we expanded the A549 experiments into serial imaging to test scission performance and visually screen for cytoxicity. Cells were stained with a SAFE647-conjugated anti-EGFR antibody, quenched/cleaved with BHQ3-N-Tz and then returned to routine culture conditions at 37 °C, with images of the same cellular area collected at each stage. After 24 h, the cells were re-imaged with live-cell and dead-cell staining dyes (live: calcein AM, dead: SYTOX Red) to determine their viability (Fig. 3b; SAFE). Cell viability readouts with PrestoBlue confirmed non-toxicity across the working time and concentration range for both SAFE-conjugated antibodies and the BHQ3-N-Tz scissors (Supplementary Fig. 4).

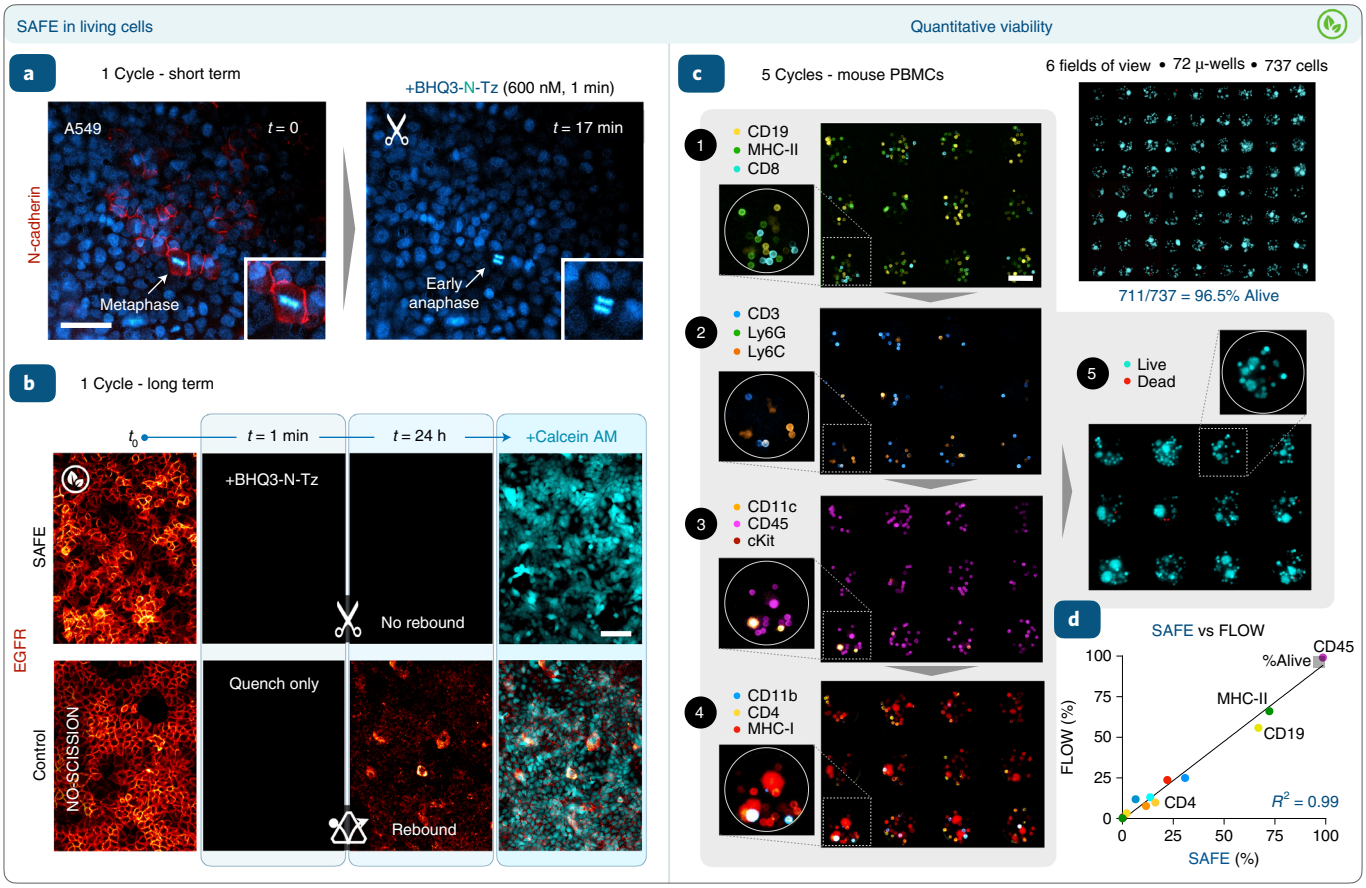

Fig. 3 | Rapid, durable and non-toxic multiplexing of living cells. a, Staining and scission with SAFE647–anti-N-cadherin confirmed efficient scission and short-term non-toxicity in living A549 cells, a subset of which progressed through mitosis during the experiment. Scale bar, 50 µm. **b**, Longer-term imaging of A549 cells was used to confirm the lack of toxicity and assess the effect of scission. Serial imaging over 24 h demonstrated durable signal elimination and intact live-cell calcein AM staining for SAFE. Control cells stained and quenched in parallel with a non-cleavable anti-EGFR fluorophore–TCO conjugate and BHQ3-Tz[33] were initially dark but exhibited marked rebound of the fluorescent signal 24 h later, likely owing to extracellular/intracellular degradation of the BHQ3 quencher, indicating a critical role for scission. Scale bar, 100 µm. **c**, To quantify cell viability across multiple cycles of staining and quenching, living mouse PBMCs were isolated, aliquoted and loaded into microwells for imaging. The cells ($n = 72$ wells) were profiled with a SAFE panel of 12 immune markers and imaged in sets of three, followed by live/dead staining dyes to assess cell survival. Efficient scission performance produced images with high signal to background across all five cycles and no evident residual signal. Scale bar, 50 µm. **d**, Both cell viability after bioorthogonal profiling (96.5% SAFE versus 96.2% FLOW) and marker abundance (% positive cells) matched well with flow cytometry controls ($R^2 = 0.99$). All experiments were repeated independently three times.

Consistent with complete scission of the quenched fluorophores, cells remained non-fluorescent on day 2, with no signal rebound observed. The cells were calcein AM-bright and had increased in density, consistent with unhindered interim proliferation. As a control, we used a conventional TCO–Tz pair that can click for bioorthogonal quenching but cannot cleave fluorophores from the antibody[33]. Although the cells were again calcein AM$^+$ and proliferating, a spontaneous increase in fluorescence signal was observed in the absence of scission (Fig. 3b; CONTROL). Black Hole Quenchers are known to be vulnerable to azo bond cleavage, particularly in vivo[38]; the observed rebound is consistent with slow intracellular and/or extracellular degradation of the BHQ3, leading to loss of quenching and the reappearing signal. Although both bioorthogonal methods achieve effective short-term cycling in living cells, scission is essential for serial profiling in longer timeframes where antibody internalization is expected and fluorescence rebound is a hazard.

We next sought to extend SAFE live-cell cycling to mixed populations of primary immune cells. To image living mouse PBMCs in suspension, we fabricated polydimethylsiloxane (PDMS) microwells (80-µm diameter, 80-µm depth) using soft lithography[39]. Both short-term imaging experiments and subsequent cell culture experiments (vide infra) were performed with these microwells, which showed excellent retention of the suspended cells, necessary for marker quantitation across cycles. Freshly harvested mouse PBMCs were isolated, pooled and then loaded into microwells for imaging, reserving aliquots for parallel analysis by flow cytometry. SAFE-labeled antibodies were compared to conventionally labeled controls to validate staining specificity (Supplementary Fig. 5). We visualized 12 targets across four cycles of imaging and quenching in live cells over the course of <2 h of elapsed time. At the end, we determined the cell viability (711 alive cells out of 737 total cells in 72 microwells, 96.5% alive) in a fifth round of imaging with calcein AM/SYTOX Red (Fig. 3c). The cells expressing each marker were counted and compared to the aliquot analyzed synchronously by flow cytometry for the same target panel. There was an excellent correlation ($R^2 = 0.985$) between populations measured by SAFE ($n = 737$) and flow cytometry ($n > 10^5$) in both their marker abundance and in the measured cell viability (96.5% by SAFE versus 96.2% by flow; Fig. 3d), confirming (1) the quantitative staining

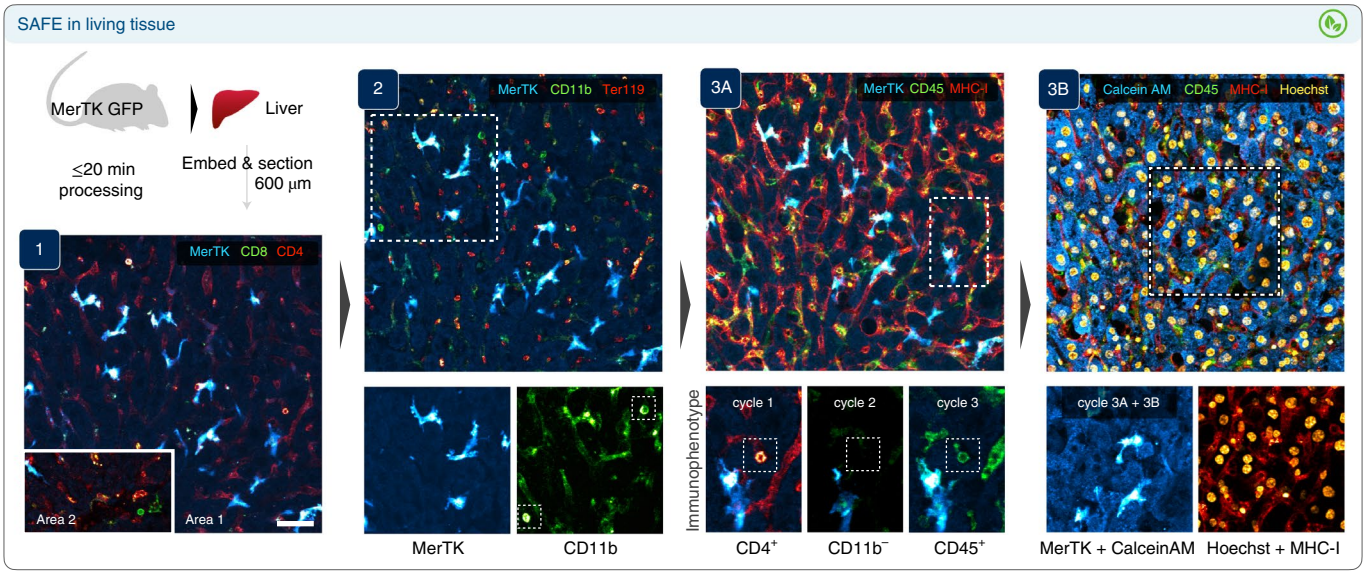

Fig. 4 | SAFE imaging of living hepatic tissue. Surgically harvested liver from a mouse bearing GFP$^+$ macrophages (MerTK-GFP) was swiftly chilled, embedded in agarose, sectioned, mounted in live-cell imaging solution at 37 °C and profiled in three cycles. Cycle 1 highlighted CD4$^+$ sinusoidal endothelium[67], bright CD4$^+$ T cells and rare CD8$^+$ T cells (area 2). After scission, cycle 2 identified CD11b$^+$ MerTK-GFP macrophages and CD11b bright immune cells (inset) as well as Ter119$^+$ red blood cells within the sinusoids. Integration of immunophenotypic data across three cycles was also feasible with cross-registration of the MerTK channel, allowing clear identification of a CD45$^+$CD4$^+$CD11b$^-$ T cell (cycle 3A). Finally, the addition of Hoechst and calcein AM (cycle 3B) enabled nuclear identification and confirmed brisk activation of the live-cell dye across the imaged living tissue section. The experiment was repeated independently two times, with two liver sections imaged per mouse and two or three regions of interest imaged per section (scale bar, 40 µm).

accuracy across multiple cycles of imaging and scission-mediated fluorophore exchange and (2) the lack of toxicity to living PBMCs.

SAFE enables cycling in living tissue. Whereas the in situ analysis of dispersed cells can reveal cellular interactions and differentiation in complex populations (vide infra), multiplexed imaging of living tissues would allow visualization of cellular dynamics within intact biological architectures. To explore the performance of SAFE in this context, we prepared freshly harvested liver slices from a Mer tyrosine kinase (MerTK)-GFP mouse[40], in which GFP$^+$ macrophages provide both a positive control for immunostaining and spatial landmarks for image focus and registration during cycling. We stained the liver section with anti-CD45 (AF555) and collected a *z*-stack time lapse (Supplementary Movie 1), capturing the migration of CD45$^+$ cells and quantifying the kinetic performance of staining and scission in living hepatic tissue. Real-time incubation of liver sections with a SAFE647-labeled anti-MHC-I antibody yielded bright cell membrane signal within minutes ($t_{1/2} = 3 \pm 0.3$ minutes); that signal was then rapidly and selectively eliminated upon click/quench scission with BHQ3-N-Tz ($t_{1/2} = 2 \pm 0.1$ minutes, 98% signal clearance) (Supplementary Fig. 6).

Expanding on these results, we went on to stain a fresh MerTK-GFP liver section with SAFE-modified antibodies (anti-CD8, CD4, CD11b, Ter119, CD45 and MHC-I) in three cycles (Fig. 4). Bright calcein AM staining at the end of imaging confirmed intact tissue viability after cycling, with Hoechst 33342 added as a nuclear reference marker for enumeration of all cells. Insets within the figure illustrate key marker staining patterns both within and across cycles, including positive/negative controls (for example, GFP$^+$, CD11b$^+$ and Ter119$^-$ macrophages), and the ability to assemble a cellular immunophenotype from successive rounds of imaging. The full multiplexed data and additional inter-cycle composite images that highlight tissue architecture are presented in Supplementary Figs. 7 and 8.

Profiling the differentiation of living bone marrow at high spatial resolution. Hematopoietic development generates phenotypic diversity as multipotent stem/progenitor cells differentiate into their repertoire of mature progeny. High-dimensional multiplexed profiling[41] and single-cell gene expression/barcoding technologies[42] have traced developmental hierarchies of hematopoietic lineages. Directly visualizing the bone marrow cells and their ensemble of surface markers amidst these changes, however, has not been possible. As an initial test of the feasibility of SAFE profiling of living bone marrow, freshly harvested murine bone marrow cells were counted and put into culture overnight. We profiled 12 immune markers (three markers per cycle, four cycles total), with a focus on myeloid precursors (Fig. 5a), using confocal imaging to distinguish membrane/cytoplasmic staining. Viability was confirmed by calcein blue AM staining with the final cycle of the profiling sequence (Supplementary Fig. 9).

CD8$^+$ cells were rare, indicating that non-adherent T cells were not well retained in this staining format. Images demonstrated the presence of erythroid (Ter119$^+$), lymphoid (CD19$^+$) and myeloid (CD11b$^+$) subsets within the population, including cells across a spectrum of functional differentiation. A continuum of CD11b, Ly6C and Ly6G expression was evident in the high-resolution composite image (Fig. 5b), with myeloid precursors (CD11b+ and Ly6C+) that render as blue/cyan and mature Ly6G$^+$ neutrophils that appear magenta/red. A subset of phagocytically proficient cells (CD14$^+$ and F4/80$^+$ in cycles 2 and 3, respectively) exhibited a pattern of multi-color intracellular staining consistent with antibody internalization before scission, in addition to the on/off cycling of specific cell surface markers. Apart from this subpopulation, negligible cytoplasmic signal was observed after four complete cycles, indicating the feasibility of accurate, iterative staining and scission in this cellular context.

To implement longitudinal bioorthogonal profiling on longer time scales—that is, across not just multiple cycles but multiple

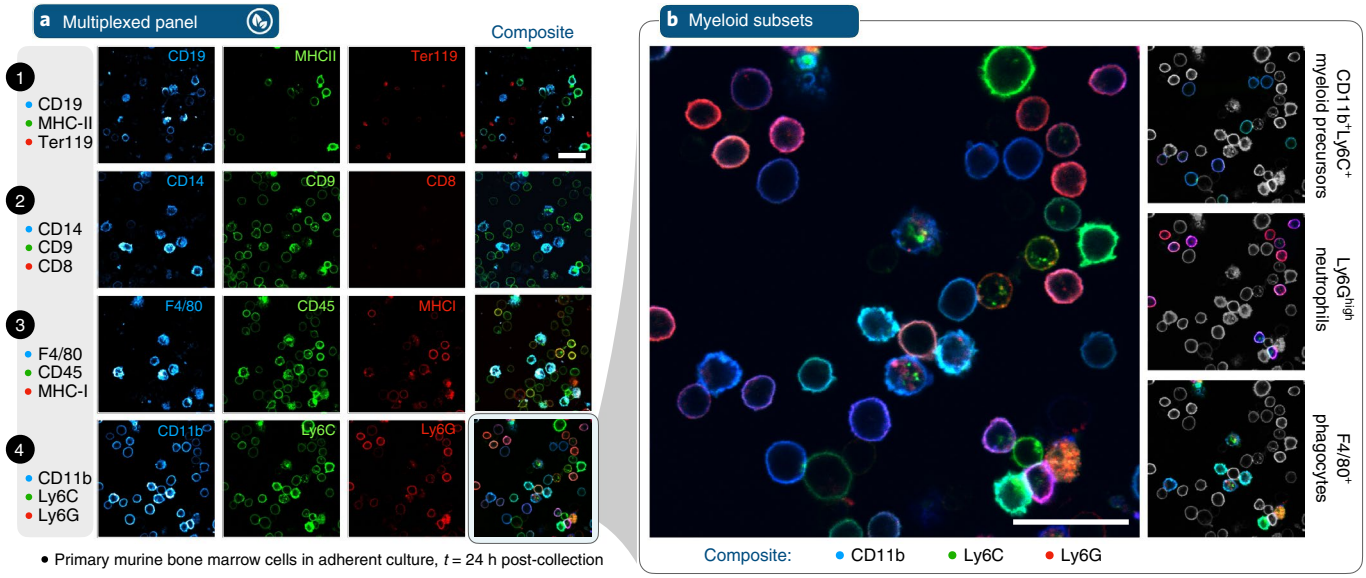

Fig. 5 | SAFE imaging of living bone marrow. a, Primary murine bone marrow cells were isolated, plated in adherent culture and imaged after 24 h. Confocal microscopy of 12 markers profiled in four cycles enabled discrimination of intracellular and extracellular fluorescent staining at high spatial resolution. A minority of cells displayed intracellular staining that was not removed by scission, suggestive of antibody internalization before fluorophore scission with BHQ3-N-Tz. Scale bar, 25 µm. **b**, A focus on the myeloid markers in cycle 4 reveals an ensemble of myeloid precursors (CD11b$^+$ and Ly6C$^+$), Ly6G-Hi neutrophils and F4/80$^+$ phagocytes (F4/80$^+$) within the developing bone marrow cell population (scale bar, 25 µm), highlighted in the selectively (de)colorized individual panels at right. Experiments were repeated independently three times.

days—we selected a model system with well-defined cellular dynamics. Estrogen-regulated Hoxb8 (ER-Hoxb8) hematopoietic progenitor cells are conditionally immortalized by retroviral infection of myeloid bone marrow progenitors[43]. Removal of β-estradiol from culture media triggers the ER-Hoxb8 differentiation program, and cells become mature neutrophils by days 4–6, a developmental sequence that has been well-characterized by flow cytometry and gene expression (Fig. 6, inset)[44]. Loss of cKit expression and sequential upregulation of CD11b, Ly6C and Ly6G occur in tandem with population expansion.

We, thus, loaded a sparse density of ER-Hoxb8 cells into PDMS microwells (width: 70 µm, height: 80 µm; Fig. 6a), fabricated as in the PBMC studies (vide supra). The same cells were imaged longitudinally during differentiation (day 0, day 2, day 4 and day 6) in two profiling cycles at each time point, staining for CD45 and F4/80 as positive/negative controls, respectively, in addition to the quartet of differentiation markers. At day 0, all cells were CD45$^+$cKit$^+$ and negative for the remaining panel, as expected. Rapid population growth by day 2 tracked with broad upregulation of CD11b and a subset of Ly6C$^+$ cells. The density of viable cells peaked on day 4, concurrently with the appearance of bright Ly6G staining. Given the short lifespan of differentiated granulocytes[45], population density had decreased slightly by day 6, consistent with the fraction of dead cells normally observed by flow cytometry. F4/80 staining remained negative throughout, as expected for differentiation under neutrophil-selective culture conditions. Cell growth during temporospatial profiling was vigorous, allowing quantitative analysis of both proliferation and differentiation across the individual microwells (Fig. 6b and Supplementary Fig. 10).

Discussion

The bioorthogonal framework of SAFE creates a new method for multiplexed longitudinal profiling of living biological samples, applied here to demonstrate nine-color imaging of murine hepatic tissue and 14-color imaging of primary hematopoietic and immune populations, across a time scale spanning minutes to days. Methods that incorporate multiple cycles of fluorescent staining and quenching were originally developed for paraffin-embedded tissue sections that can withstand harsh destaining conditions[12,46,47]. We and others have subsequently developed gentler DNA-barcoded antibody technologies for cellular profiling[14,15,48–50], but these, too, require long destaining times and solvent/buffer conditions incompatible with live-cell analysis. Our recent method for immunostaining with Tz–TCO-driven bioorthogonal quenching[33,51] achieves its speed by circumventing the need to remove fluorophores. Although capable of rapid temporal cycling at non-toxic reagent concentrations, the quenching is reversed by biochemical degradation over longer timeframes in living systems, leading to signal rebound (Fig. 3b; control). In contradistinction, the SAFE method bypasses the above shortcomings and allows efficient, durable cycling (>99% signal clearance in <30 s; Fig. 2d) while using nanomolar concentrations of reagents for gentle and irreversible fluorophore scission. By accelerating the scission sequence with cooperative BHQ3–fluorophore interactions, the SAFE reagents achieve a unique combination of intrinsic biochemical stability (C_2TCO, >97% intact at 48 h) and high reactivity that arises as an emergent property of the system. To our knowledge, SAFE is currently the only technique that allows such temporospatial profiling in living cells and tissues.

Bioorthogonal reactions have long been described in live cells as an alternative route to biomolecular tagging[52], with incorporation of functionalized non-canonical amino acids into proteins[53,54], modified nucleosides into DNA/RNA[55], metabolic building blocks into glycans[56] or clickable tags into chemical probes[57,58], followed by subsequent click-mediated labeling. The impetus for developing these strategies has primarily been visualization of the different classes of biomolecules in living systems, exploiting the small footprint of compact chemical tags for tracking[56] or creating a readout for replication/metabolism[55]. Such tags have also featured in strategies for super-resolution microscopy[59–61]. Here, we apply chemical tools not to deliver labels but, rather, to remove them via bioorthogonal bond cleavage[62,63], pursuing multiplexed temporal analysis of cell surface protein expression.

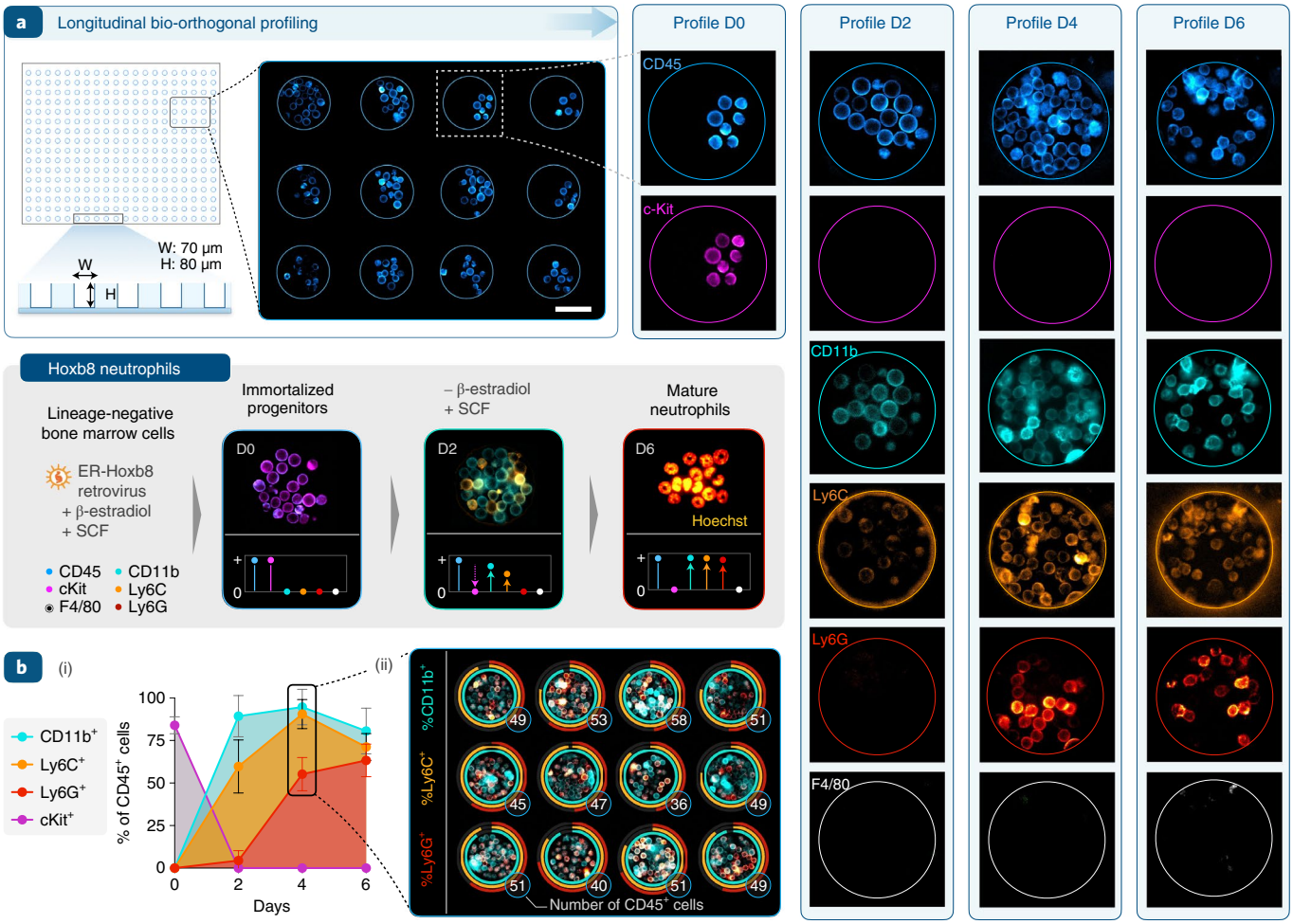

Fig. 6 | Longitudinal profiling of neutrophil differentiation. a, Deep PDMS microwells retain suspension cells in culture for serial imaging. Scale bar, 50 µm. Bone-marrow-derived ER-Hoxb8 cells are conditionally immortalized when cultured with β-estradiol; removal of β-estradiol triggers synchronous expansion and neutrophilic differentiation. This developmental sequence induces broad changes in extracellular marker expression and cellular morphology (gray panel, inset). To track this process, CD45, cKit, CD11b, Ly6C, Ly6G and F4/80 were serially profiled at days 0, 2, 4 and 6, before and during differentiation. CD45 (positive control) and F4/80 (negative control) expression was stable, whereas cKit (a progenitor cell marker) expression quickly decreased, disappearing after day 0. As expected, the fraction of cells expressing CD11b, Ly6C and Ly6G rose in sequence over the first 4–6 days. **b**, Quantitative expression of differentiation markers across 6 days and four profiles: (1) averaged across a set of $n = 12$ microwells (plotted as mean, s.d.); and (2) quantified on day 4 to track proliferation and variation across individual microwells. Ring plots track marker expression (fraction of positive cells, encoded by color) and the total number of CD45⁺ cells per well (in white). D, day; H, height; W, width.

Although non-lethal methods for intracellular antibody delivery have been explored[64–66], such tools are not yet compatible with routine immunostaining or the construction of multiplexed panels; these limitations currently restrict SAFE multiplexed profiling of living cells and tissues to extracellular markers. Likewise, the present iteration of the SAFE chemistry relies on diffusion for clearance of the cleaved dye, a facile process with cell surface targets but less straightforward for hydrophilic, membrane-impermeable fluorophores released within the cytoplasm. Membrane permeability of BHQ3–Tz scissors (or other bioorthogonal scission machinery) would also need to be further defined. Differences in the speed of scission/signal clearance within tissues relative to cells (Supplementary Fig. 6) are another area for future study and suggest an opportunity for orientation-controlled cleavage as a mechanism to release only dark fluorophores (Supplementary Fig. 2a, scenario II).

The proof-of principle experiments shown here can be further expanded to increase the number of cycles and targets within each profile, assembling broader marker panels for study of complex living tissues, especially in immunologically complex environments, such as lymph node, tonsil, spleen or tumor tissue. Observed scission efficiencies of >99.5% for cells and ~98% in tissue should permit more than 12 cycles of multiplexing at robust signal–background ratios (Supplementary Fig. 1b). One of the key advantages of the SAFE method is that the underlying bioorthogonal scission reaction is compatible with any conjugatable dye, including polymeric fluorochromes (for example, the BV dye series), that are otherwise difficult to quench. Because a range of bright polymer dyes can be excited in the violet/UV, their use together with organic rhodamine/cyanine dyes could enable broader multiplexing of up to ~8 channels per cycle with minimal spectral overlap. In this mode, the potential ability of BHQ3–BV dye interactions to accelerate the click/scission reactions awaits study, but forthcoming developments in Tz–TCO scission chemistry will also provide an alternative. Finally, although our focus here was on demonstrating temporospatial analysis in well-defined model systems, the above approaches open the door to multiplexed functional profiling and longitudinal observation of a broad range of living cells and tissues, immediately after explantation or even in vivo.

Online content

Any methods, additional references, Nature Research reporting summaries, source data, extended data, supplementary information, acknowledgements, peer review information; details of author contributions and competing interests; and statements of data and code availability are available at https://doi.org/10.1038/s41587-022-01339-6.

Received: 1 October 2021; Accepted: 28 April 2022;
Published online: 02 June 2022

References

1. Sullivan, Z. A. et al. γδ T cells regulate the intestinal response to nutrient sensing. *Science* **371**, eaba8310 (2021).
2. Patriarchi, T. et al. An expanded palette of dopamine sensors for multiplex imaging in vivo. *Nat. Methods* **17**, 1147–1155 (2020).
3. Costantini, L. M. et al. A palette of fluorescent proteins optimized for diverse cellular environments. *Nat. Commun.* **6**, 7670 (2015).
4. Rodriguez, E. A. et al. The growing and glowing toolbox of fluorescent and photoactive proteins. *Trends Biochem. Sci.* **42**, 111–129 (2017).
5. Polonsky, M. et al. Induction of CD4 T cell memory by local cellular collectivity. *Science* **360**, eaaj1853 (2018).
6. Arlauckas, S. P. et al. In vivo imaging reveals a tumor-associated macrophage-mediated resistance pathway in anti-PD-1 therapy. *Sci. Transl. Med.* **9**, eaal3604 (2017).
7. Zindel, J. et al. Primordial GATA6 macrophages function as extravascular platelets in sterile injury. *Science* **371**, eabe0595 (2021).
8. Alon, S. et al. Expansion sequencing: spatially precise in situ transcriptomics in intact biological systems. *Science* **371**, eaax2656 (2021).
9. Cho, C. S. et al. Microscopic examination of spatial transcriptome using Seq-Scope. *Cell* **184**, 3559–3572 (2021).
10. Eng, C. L. et al. Transcriptome-scale super-resolved imaging in tissues by RNA seqFISH. *Nature* **568**, 235–239 (2019).
11. Stickels, R. R. et al. Highly sensitive spatial transcriptomics at near-cellular resolution with Slide-seqV2. *Nat. Biotechnol.* **39**, 313–319 (2021).
12. Lin, J. R., Fallahi-Sichani, M. & Sorger, P. K. Highly multiplexed imaging of single cells using a high-throughput cyclic immunofluorescence method. *Nat. Commun.* **6**, 8390 (2015).
13. Goltsev, Y. et al. Deep profiling of mouse splenic architecture with CODEX multiplexed imaging. *Cell* **174**, 968–981 (2018).
14. Guo, S. M. et al. Multiplexed and high-throughput neuronal fluorescence imaging with diffusible probes. *Nat. Commun.* **10**, 4377 (2019).
15. Saka, S. K. et al. Immuno-SABER enables highly multiplexed and amplified protein imaging in tissues. *Nat. Biotechnol.* **37**, 1080–1090 (2019).
16. Radtke, A. J. et al. IBEX: a versatile multiplex optical imaging approach for deep phenotyping and spatial analysis of cells in complex tissues. *Proc. Natl Acad. Sci. USA* **117**, 33455–33465 (2020).
17. Angelo, M. et al. Multiplexed ion beam imaging of human breast tumors. *Nat. Med.* **20**, 436–442 (2014).
18. Bendall, S. C. et al. Single-cell mass cytometry of differential immune and drug responses across a human hematopoietic continuum. *Science* **332**, 687–696 (2011).
19. Jackson, H. W. et al. The single-cell pathology landscape of breast cancer. *Nature* **578**, 615–620 (2020).
20. Hartmann, F. J. & Bendall, S. C. Immune monitoring using mass cytometry and related high-dimensional imaging approaches. *Nat. Rev. Rheumatol.* **16**, 87–99 (2020).
21. Mahdessian, D. et al. Spatiotemporal dissection of the cell cycle with single-cell proteogenomics. *Nature* **590**, 649–654 (2021).
22. Stoeckius, M. et al. Simultaneous epitope and transcriptome measurement in single cells. *Nat. Methods* **14**, 865–868 (2017).
23. McKinnon, K. M. Flow cytometry: an overview. *Curr. Protoc. Immunol.* **120**, 5.1.1–5.1.11 (2018).
24. Giannone, G. et al. Dynamic superresolution imaging of endogenous proteins on living cells at ultra-high density. *Biophys. J.* **99**, 1303–1310 (2010).
25. Strauss, S. & Jungmann, R. Up to 100-fold speed-up and multiplexing in optimized DNA-PAINT. *Nat. Methods* **17**, 789–791 (2020).
26. Bechtel, T. J., Reyes-Robles, T., Fadeyi, O. O. & Oslund, R. C. Strategies for monitoring cell-cell interactions. *Nat. Chem. Biol.* **17**, 641–652 (2021).
27. Jenkins, R. W. et al. Ex vivo profiling of PD-1 blockade using organotypic tumor spheroids. *Cancer Discov.* **8**, 196–215 (2018).
28. Voabil, P. et al. An ex vivo tumor fragment platform to dissect response to PD-1 blockade in cancer. *Nat. Med.* **27**, 1250–1261 (2021).
29. Engblom, C. et al. Osteoblasts remotely supply lung tumors with cancer-promoting SiglecF^{high} neutrophils. *Science* **358**, eaal5081 (2017).
30. Katzenelenbogen, Y. et al. Coupled scRNA-seq and intracellular protein activity reveal an immunosuppressive role of TREM2 in cancer. *Cell* **182**, 872–885 (2020).
31. Pfirschke, C. et al. Tumor-promoting Ly-6G^{+} SiglecF^{high} cells are mature and long-lived neutrophils. *Cell Rep.* **32**, 108164 (2020).
32. Pucella, J. N., Upadhaya, S. & Reizis, B. The source and dynamics of adult hematopoiesis: insights from lineage tracing. *Annu. Rev. Cell Dev. Biol.* **36**, 529–550 (2020).
33. Ko, J., Oh, J., Ahmed, M. S., Carlson, J. C. T. & Weissleder, R. Ultra-fast cycling for multiplexed cellular fluorescence imaging. *Angew. Chem. Int. Ed. Engl.* **59**, 6839–6846 (2020).
34. Nguyen, S. S. & Prescher, J. A. Developing bioorthogonal probes to span a spectrum of reactivities. *Nat. Rev. Chem.* **4**, 476–489 (2020).
35. Carlson, J. C. T., Mikula, H. & Weissleder, R. Unraveling tetrazine-triggered bioorthogonal elimination enables chemical tools for ultrafast release and universal cleavage. *J. Am. Chem. Soc.* **140**, 3603–3612 (2018).
36. Sarris, A. J. C. et al. Fast and pH-independent elimination of *trans*-cyclooctene by using aminoethyl-functionalized tetrazines. *Chemistry* **24**, 18075–18081 (2018).
37. Wilkovitsch, M. et al. A cleavable C_2-symmetric *trans*-cyclooctene enables fast and complete bioorthogonal disassembly of molecular probes. *J. Am. Chem. Soc.* **142**, 19132–19141 (2020).
38. Linder, K. E. et al. Synthesis, in vitro evaluation, and in vivo metabolism of fluor/quencher compounds containing IRDye 800CW and Black Hole Quencher-3 (BHQ-3). *Bioconjug. Chem.* **22**, 1287–1297 (2011).
39. Zaretsky, I. et al. Monitoring the dynamics of primary T cell activation and differentiation using long term live cell imaging in microwell arrays. *Lab Chip* **12**, 5007–5015 (2012).
40. Mohan, J. F. et al. Imaging the emergence and natural progression of spontaneous autoimmune diabetes. *Proc. Natl Acad. Sci. USA* **114**, E7776–E7785 (2017).
41. Qiu, P. et al. Extracting a cellular hierarchy from high-dimensional cytometry data with SPADE. *Nat. Biotechnol.* **29**, 886–891 (2011).
42. Loughran, S. J., Haas, S., Wilkinson, A. C., Klein, A. M. & Brand, M. Lineage commitment of hematopoietic stem cells and progenitors: insights from recent single cell and lineage tracing technologies. *Exp. Hematol.* **88**, 1–6 (2020).
43. Wang, G. G. et al. Quantitative production of macrophages or neutrophils ex vivo using conditional Hoxb8. *Nat. Methods* **3**, 287–293 (2006).
44. Sykes, D. B. et al. Inhibition of dihydroorotate dehydrogenase overcomes differentiation blockade in acute myeloid leukemia. *Cell* **167**, 171–186 (2016).
45. Hidalgo, A., Chilvers, E. R., Summers, C. & Koenderman, L. The neutrophil life cycle. *Trends Immunol.* **40**, 584–597 (2019).
46. Gerdes, M. J. et al. Highly multiplexed single-cell analysis of formalin-fixed, paraffin-embedded cancer tissue. *Proc. Natl Acad. Sci. USA* **110**, 11982–11987 (2013).
47. Schubert, W. et al. Analyzing proteome topology and function by automated multidimensional fluorescence microscopy. *Nat. Biotechnol.* **24**, 1270–1278 (2006).
48. Ullal, A. V. et al. Cancer cell profiling by barcoding allows multiplexed protein analysis in fine-needle aspirates. *Sci. Transl. Med.* **6**, 219ra9 (2014).
49. Agasti, S. S., Liong, M., Peterson, V. M., Lee, H. & Weissleder, R. Photocleavable DNA barcode–antibody conjugates allow sensitive and multiplexed protein analysis in single cells. *J. Am. Chem. Soc.* **134**, 18499–18502 (2012).
50. Giedt, R. J. et al. Single-cell barcode analysis provides a rapid readout of cellular signaling pathways in clinical specimens. *Nat. Commun.* **9**, 4550 (2018).
51. Oh, J. et al. Rapid serial immunoprofiling of the tumor immune microenvironment by fine needle sampling. *Clin. Cancer Res.* **27**, 4781–4793 (2021).
52. Prescher, J. A. & Bertozzi, C. R. Chemistry in living systems. *Nat. Chem. Biol.* **1**, 13–21 (2005).
53. de la Torre, D. & Chin, J. W. Reprogramming the genetic code. *Nat. Rev. Genet.* **22**, 169–184 (2021).
54. Lang, K. & Chin, J. W. Cellular incorporation of unnatural amino acids and bioorthogonal labeling of proteins. *Chem. Rev.* **114**, 4764–4806 (2014).
55. Salic, A. & Mitchison, T. J. A chemical method for fast and sensitive detection of DNA synthesis in vivo. *Proc. Natl Acad. Sci. USA* **105**, 2415–2420 (2008).
56. Palaniappan, K. K. & Bertozzi, C. R. Chemical glycoproteomics. *Chem. Rev.* **116**, 14277–14306 (2016).
57. Cañeque, T., Müller, S. & Rodriguez, R. Visualizing biologically active small molecules in cells using click chemistry. *Nat. Rev. Chem.* **2**, 202–215 (2018).
58. Yang, K. S., Budin, G., Tassa, C., Kister, O. & Weissleder, R. Bioorthogonal approach to identify unsuspected drug targets in live cells. *Angew. Chem. Int. Ed. Engl.* **52**, 10593–10597 (2013).
59. Nikić, I. et al. Minimal tags for rapid dual-color live-cell labeling and super-resolution microscopy. *Angew. Chem. Int. Ed. Engl.* **53**, 2245–2249 (2014).
60. Beliu, G. et al. Bioorthogonal labeling with tetrazine-dyes for super-resolution microscopy. *Commun. Biol.* **2**, 261 (2019).
61. Werther, P. et al. Live-cell localization microscopy with a fluorogenic and self-blinking tetrazine probe. *Angew. Chem. Int. Ed. Engl.* **59**, 804–810 (2020).

62. Versteegen, R. M., Rossin, R., ten Hoeve, W., Janssen, H. M. & Robillard, M. S. Click to release: instantaneous doxorubicin elimination upon tetrazine ligation. *Angew. Chem. Int. Ed. Engl.* **52**, 14112–14116 (2013).
63. Wang, J., Wang, X., Fan, X. & Chen, P. R. Unleashing the power of bond cleavage chemistry in living systems. *ACS Cent. Sci.* **7**, 929–943 (2021).
64. Singh, K., Ejaz, W., Dutta, K. & Thayumanavan, S. Antibody delivery for intracellular targets: emergent therapeutic potential. *Bioconjug. Chem.* **30**, 1028–1041 (2019).
65. Canton, I. et al. Fully synthetic polymer vesicles for intracellular delivery of antibodies in live cells. *FASEB J.* **27**, 98–108 (2013).
66. Röder, R. et al. Intracellular delivery of nanobodies for imaging of target proteins in live cells. *Pharm. Res.* **34**, 161–174 (2017).
67. Scoazec, J. Y. & Feldmann, G. Both macrophages and endothelial cells of the human hepatic sinusoid express the CD4 molecule, a receptor for the human immunodeficiency virus. *Hepatology* **12**, 505–510 (1990).

Methods

Chemistry. *Synthesis and characterization.* Detailed synthetic methods and characterization data are presented in full in the Supplementary Information, including probe activation, bioorthogonal click and scission kinetics, nuclear magnetic resonance spectra and electrospray ionization mass spectrometry data.

Bioconjugation and routine imaging methods/controls. *Antibodies.* BSA-free antibodies were purchased from established vendors and stored according to manufacturer recommendations. Cetuximab (anti-EGFR antibody, Erbitux) was used to optimize staining and quenching/scission methods. Antibodies used for all SAFE imaging throughout the study are tabulated in Supplementary Table 1. All antibodies were validated with conventional immunofluorescence imaging (secondary antibody staining) on positive cell lines or mouse splenocytes before usage in SAFE imaging.

Antibody modification with SAFE probes. For functionalization with fluorophore–C_2TCO conjugates, antibodies were first exchanged from their storage solution into PBS-bicarbonate buffer (PBS supplemented with 100 mM sodium bicarbonate, pH 8.4) using a 40K Zeba Spin column (Thermo Fisher Scientific, 87765). After buffer exchange, antibodies were incubated with a 4–8-fold molar excess of the activated dye-C_2TCO-NHS linker for 25 minutes at room temperature. The completed conjugation reaction was loaded onto another 40K Zeba column (equilibrated with PBS) for desalting and removal of unreacted dye molecules. The absorbance spectrum of the conjugated antibody was measured using a NanoDrop 1000 (Thermo Fisher Scientific) to determine the degree of labeling (DOL), applying the known extinction coefficients of the dye, IgG antibody and standard correction factor (CF280) for the dye absorbance at 280 nm. The SAFE-conjugated antibodies were stored in the dark at 4 °C in PBS until usage.

Immunostaining and fluorophore scission. Cells were cultured as specified (vide infra), stained with 5 μg ml^{-1} of SAFE probes and incubated for 10 minutes at 4 °C. Hoxb8 cells were first blocked with 0.5% BSA-PBS for 10 minutes at 4 °C before staining. Cetuximab staining of A549 and A431 cells is indistinguishable with or without blocking, so no pretreatment was applied. After imaging, a 500-nM or 600-nM solution of BHQ3-N-Tz (**2**) diluted in PBS was used to wash cells for quenching and scission. Although signal removal is characteristically complete in 30–60 s, we used a routine interval of up to 3–5 minutes to ensure complete removal of residual fluorescence. For the longitudinal imaging kinetics (Fig. 2d), cells were serially imaged during the click/scission process to quantify the aggregate quench/scission rates (Supplementary Fig 3). In routine experiments, the cells and remaining BHQ3-N-Tz were washed three times after incubation with PBS in immediate succession. After quenching/scission, the staining, imaging and scission cycle was repeated for multiplexed protein profiling of the same cells. Imaging was performed in Live Cell Imaging Solution (Thermo Fisher Scientific, A14291DJ). Calcein AM (Thermo Fisher Scientific, C1430) and SYTOX Red (Thermo Fisher Scientific, S34859) were used for live-cell and dead-cell staining, and Hoechst 33342 (Thermo Fisher Scientific, H3570) was used for nuclear staining in a subset of experiments. Hoechst staining was associated with an increased rate of phototoxic stress in live-cell microscopy, especially in longitudinal imaging, so its use was reserved for short-term experiments and for those in which nuclear morphology was particularly relevant and necessary.

Longitudinal acquisition—photobleaching control. A431 cells were stained with 5 μg ml^{-1} of SAFE647-conjugated cetuximab for 10 minutes at room temperature and then washed three times with PBS (5–10 s each). Images were then acquired every 5 s at experimental conditions (illumination intensity, exposure time and microscope) matched to those of Fig. 2d. As illustrated by the images and intensity profiles at selected time points in Supplementary Fig. 3, no measurable photobleaching was observed.

SAFE specificity. To verify that staining accuracy is not affected by the bioorthogonally cleavable linker, SAFE-modified antibodies were compared to conventionally labeled controls. A representative panel of anti-CD11b (MB488), CD45 (AF555), CD8 (MB594) and Ly6G (AF647) antibodies were modified with individual SAFE probes, as specified. In parallel, control antibodies in a non-overlapping color/channel were prepared via conventional activated ester labeling. AZDye 555 NHS ester (Fluoroprobes, 1166-5) was used to label anti-CD11b, whereas AFDye 488 TFP ester (Fluoroprobes, 1026-5) was used to label the parent anti-CD45, CD8 and Ly6G antibodies. Control antibodies with a degree of labeling (DOL) of 2–3 fluorophores per antibody were prepared to match the DOL of SAFE-modified antibodies. Control and SAFE-modified antibodies (each at 5 μg ml^{-1}) were then premixed and co-incubated with mouse splenocytes for 10 minutes at room temperature. After washing three times with PBS (5–10 s each), the stained cells were imaged on μ-Slide 8 Well Glass Bottom slides (Ibidi, 80826) using a DeltaVision inverted fluorescence microscope (Supplementary Fig. 5).

Fluorescent imaging and analysis. An Olympus BX-63 upright automated epifluorescence microscope and a DeltaVision inverted fluorescence microscope were used to acquire fluorescent images. DAPI, FITC, TxRed/Cy3 and Cy5 filter cubes were used to excite calcein AM live-cell stains and AF488, AF594 and AF647 fluorophores, respectively. ImageJ was used to measure fluorescent intensities in cells.

Cell culture methods. *Cell line culture.* The A549 (CCL-185) and A431 (CRL-1555) cell lines were purchased from the American Type Culture Collection (ATCC) and used in method development experiments. A549 cells were passaged in F-12K (ATCC, 30-2004) with 10% FBS and 1% penicillin–streptomycin according to the specifications from ATCC. Cells were first grown in a 150-mm cell culture dish and then seeded on μ-Slide 8 Well Glass Bottom slides for imaging. After 24–48 h, confluency was assessed, and cells were stained and imaged.

Cytotoxicity assays. A431 cells were first seeded on 96-well plates at a density of ~10,000 cells per well. After 48 h of culture (DMEM), baseline cell viability was benchmarked using the PrestoBlue Cell Viability Reagent (Thermo Fisher Scientific, A13262) to control for any well-to-well variability in post-seeding proliferation. The cells were washed with fresh DMEM after the PrestoBlue measurement and then incubated with BHQ3-N-Tz (0–10 μM) in cell culture media. DMSO control wells were prepared to match the DMSO content (0.42%) of the 10 μM BHQ3-N-Tz sample. For the remaining reagent concentrations, media alone was used as the control, given minimal DMSO content (<0.13%). A continuous exposure of 1 hour at 37 °C was selected, corresponding to the cumulative duration of 12–20 cycles of quenching/scission (3–5 minutes each). In parallel, a separate set of cells was incubated in DMEM with 5 μg ml^{-1} of cetuximab-SAFE647 or conventionally labeled cetuximab-AF647 as a control. Media were exchanged after incubation, and the cells were returned to culture for 24 h. Cell viability was then measured with the PrestoBlue assay, with the data normalized to the baseline values from the start of the experiment (Supplementary Fig. 4).

Microwell fabrication. The microwells used to culture and/or image non-adherent cells were fabricated at the Soft Materials Cleanroom, Harvard Center for Nanoscale Systems. Each microwell array consists of 1,681 total wells. The microwells (mask design width: 60 μm, height: 80 μm) were made using soft lithography with SU-8 3050. Different widths were tested (60 μm, 80 μm and 100 μm), and 60 μm was chosen, a dimension that demonstrated no detectable cell loss throughout multiple experimental steps (for example, media change, incubation, washing and culture). PDMS was spin-coated on a patterned wafer, cured in 65 °C for 1 hour, peeled off from the wafer and then transferred to μ-Slide 8 Well Glass Bottom slides for cell culture and imaging.

Longitudinal imaging of A549 cells. *SAFE labeling.* A549 cells were cultured in μ-Slide 8 Well Glass Bottom slides for 24–48 h before imaging. After 24–48 h, cells were stained with 5 μg ml^{-1} of SAFE-conjugated (AF647) anti-EGFR antibody for 10 minutes at room temperature and then rinsed with three successive washes of PBS, culminating with the addition of live-cell imaging solution (Thermo Fisher Scientific, A14291DJ). After image acquisition, quenching was performed by incubating the stained live cells with BHQ3-N-Tz (**2**) at 600 nM. Fluorescent images were acquired after staining, 1 minute after quenching/scission and 24 h after scission. After 24 h, cells were stained with calcein AM (Thermo Fisher Scientific, C1430) and SYTOX Red (Thermo Fisher Scientific, S34859) to check cell viability. A DeltaVision inverted fluorescence microscope was used to acquire all the fluorescent images in this study.

No scission control experiments. A549 cells were cultured and prepared as above and then stained with 5 μg ml^{-1} of AF647–rTCO-conjugated (FAST647, Ko et al.[33]) anti-EGFR antibody for 10 minutes at room temperature. This antibody can click with a BHQ3–Tz quencher, but the linker/dye remains permanently attached to the antibody—that is, no scission is possible, only quenching. After image acquisition, the stained live cells were incubated with the non-scissile BHQ3-Tz (600 nM, 1 minute), as previously described. Fluorescent images were acquired after staining, 5 minutes after quenching and 24 h after quenching to quantify rebound. After imaging at 24 h, cells were stained with calcein AM (Thermo Fisher Scientific, C1430) and SYTOX Red (Thermo Fisher Scientific, S34859) to check cell viability.

SAFE Imaging of mouse PBMCs (Fig. 3c). *Ethics and veterinary care.* Oversight for this and subsequent animal experiments was provided by the Institutional Animal Care and Use Committee for Massachusetts General Hospital and Shriner's Hospital, approved under animal protocols 2013N000157 (murine tissue harvest and imaging) and 2017N000255 (murine bone marrow harvest and culture). Mice were housed at an ambient temperature of 68–73 °F, with 30–70% humidity; the light/dark cycle was 12 h light (7:00–19:00) and 12 h dark (19:00–7:00).

Mouse PBMC isolation. Whole blood was collected from C57BL/6J mice (Jackson Laboratory) by cardiac puncture. PBMCs were isolated by density gradient centrifugation. Lymphoprep (Stem Cell Technologies, 07801) was used as density gradient medium. Whole blood was diluted with an equal volume of PBS with 2% FBS, layered with Lymphoprep on top, and centrifuged at 800*g* for 20 minutes at room temperature with break off. The upper plasma layer was discarded, and the cloudy mononuclear cell layer was gently collected in a separate tube. Collected cells were washed with PBS and then cultured for imaging.

SAFE imaging in microwells. Isolated mouse PBMCs were diluted in PBS to provide an average of ten cells per well and loaded to microwell arrays for cycling and imaging. For each cycle, cells were stained with a cocktail of three SAFE antibodies (5 μg ml^{-1}) conjugated to three different fluorophores (AF488, AF594 and AF647) for 10 minutes at room temperature. Standard scission conditions used (**2**) (600 nM) for 1–3 minutes. For the 5th cycle, cells were stained with calcein AM (Thermo Fisher Scientific, C1430) and SYTOX Red (Thermo Fisher Scientific, S34859) per the vendor protocol to check cell viability after the cumulative profiling experiment. Staining and quenching solutions were diluted in PBS, and imaging was performed with cells in live-cell imaging solution (Thermo Fisher Scientific, A14291DJ). Images were acquired using a DeltaVision inverted fluorescence microscope to capture six fields of view (72 microwells). Cells were counted in ImageJ, and results were tabulated in Microsoft Excel (version 16.53) and/or Numbers (Apple, version 10.0).

Flow cytometry control experiments. Mouse PBMCs were incubated with TrueStain FcX antibody (clone 93, BioLegend) in PBS with 2% FBS before staining with antibodies directly conjugated to fluorophores. Cells were divided into two tubes to stain for myeloid markers (CD11b, CD11c, Ly6C, Ly6G, MHC-I and MHC-II) or lymphoid markers (CD3, CD4, CD8, CD19 and c-kit). Antibodies are summarized in Supplementary Table 2. DAPI was used to exclude dead cells from analysis. Cells were washed and strained through a 40-μm filter (BD Falcon, 352340) after staining and analyzed on a BD LSRII flow cytometer. AbC Total Antibody Compensation Bead Kit (Thermo Fisher Scientific, A10513) was used for single-color compensation. Flow cytometry data were then analyzed using FlowJo software (version 10.8.0, Becton Dickinson) to quantify the frequency of cells positive for each marker; the gating strategy is outlined in Supplementary Fig. 11. Lymphoprep centrifugation is selective for T, B, NK and monocyte populations and excludes granulocytes, consistent with the observed low abundance of those myeloid markers (for example, Ly6G^{+}) in the cells analyzed. Percentages (SAFE, FLOW) of positive cells for each marker are c-Kit (0.5%, 0.9%), CD8 (13.7%, 13.1%), CD11c (2.1%, 3.2%), CD19 (66.9%, 55.8%), CD45 (98.6%, 99.1%), CD11b (6.5%, 11.9%), CD4 (16.2%, 9.9%), CD3 (30.8%, 25%), MHC-II (72.3%, 66.1%), MHC-I (22.1%, 23.7%), Ly6G (0.0%, 0.2%) and Ly6C (11.6%, 7.7%).

Live tissue imaging. *Specimen preparation.* Freshly harvested liver from a Mer tyrosine kinase (MerTK)-GFP mouse was embedded in 2.5% agarose and immediately sectioned with a vibrating microtome (VF-310-0Z-VM, Precisionary Instruments). The sample and the immersion bath solution were kept at 4 °C during the entire slicing procedure. Slices of 500-μm and 700-μm thickness were obtained with optimal sectioning parameters set to 3 and 6 for the advance and oscillation speed, respectively, and then kept in cold media on ice until imaging. The living tissue sections were affixed to a glass slide with a small dab of cyanoacrylate adhesive. The slide was then mounted on a heated stage (37 °C) on a custom-made Olympus FV1000 confocal multi-photon system and imaged using a ×20 XLUMPLFLN water immersion objective (NA = 1.0, Olympus America).

Real-time tissue staining/scission. A freshly cut slice was stained with anti-CD45 (AF555) at 5 μg ml^{-1} for 5 minutes at room temperature and then rinsed three times (5–10 s each) with live-cell imaging solution (Thermo Fisher Scientific, A14291DJ). The tissue slice was then immersed in live-cell imaging solution and monitored longitudinally in the MerTK-GFP, CD45-AF555 and 647 channels. After 36.5 minutes of acquisition (*z*-stack, 15 planes, 4-μm spacing, frame interval 134.6 s), the live tissue was stained with a SAFE647-modified anti-MHC-I antibody for 11 minutes (5 μg ml^{-1} in live-cell imaging solution), followed by addition of BHQ3-N-Tz (1 μM, t = 47 minutes) for real-time scission while imaging (Supplementary Fig. 6 and Supplementary Movie 1). Quantitative kinetic analyses were derived from intensity profiles (pixel brightness versus coordinate) calculated in ImageJ and exported to GraphPad Prism for descriptive statistics. Mean and 95th percentile intensity data for each intensity profile were plotted as a function of time, with staining/scission kinetics synchronized to the time of antibody addition and BHQ3-N-Tz addition, respectively (Supplementary Fig. 6). The observed rates were used to guide the design of subsequent multiplexing.

Tissue multiplexing. Experiments were conducted by staining the live MerTK-GFP liver tissue with anti-CD4 (SAFE647) and anti-CD8 (SAFE555) antibodies (cycle 1); anti-CD11b (SAFE555) and Ter119 (SAFE647) antibodies (cycle 2); and anti-CD45 (SAFE555) and anti-MHC-I (SAFE647) antibodies (cycle 3A). For cycle 3B, calcein AM (4 μM, Thermo Fisher Scientific, C1430) and Hoechst 33342 (32.4 μM, Thermo Fisher Scientific, H3570) were added to the already-labeled tissue. For staining, the tissue was incubated with SAFE-labeled antibodies (5 μg ml^{-1}, 6 minutes) in live-cell imaging solution and washed three times (5–10 s each) with PBS before imaging in fresh live-cell imaging solution. For scission, the liver section was immersed in BHQ3-N-Tz (1 μM in PBS) for 15–20 minutes to allow for tissue penetration, click reaction, scission and optimal diffusion/clearance of the cleaved fluorophores from the tissue, as derived from kinetic studies above. The tissue was then washed three times with PBS (5–10 s each) before application of the antibody solution for the next staining cycle (see also Supplementary Figs. 7 and 8).

Mouse bone marrow imaging. *Mouse bone marrow isolation and culture.* Microcentrifuge tubes (0.5 ml) were prepared by removing the lids (scissors) and piercing a hole through the bottom of the tube using a 16-gauge sterile needle. Wild-type mice (C57BL/6J females, age 10–12 weeks) were euthanized by carbon dioxide asphyxiation, and the femurs were removed in sterile fashion. The distal end of the femur was opened using scissors, and the femur was placed with the open end facing down into the bottom of the 0.5-ml microcentrifuge tube. This tube was placed inside a 1.5-ml microcentrifuge tube, and the tube-within-a-tube was centrifuged at 10,000*g* for 15 s to 'spin-flush' the bone marrow. The 0.5-ml microcentrifuge tube and 'empty' femurs were discarded, and the bone marrow pellet (~25 μl) was resuspended in PBS containing 2% FBS and 1 mM EDTA. Mononuclear cells were enumerated by staining a small aliquot with acridine orange (Thermo Fisher Scientific, A3568) and counting using a fluorescence-based cell counter (Cellometer, Nexcelom).

Primary murine bone marrow cells were cultured in μ-Slide 8 Well Glass Bottom slides for 24 h in RPMI1640 media with glutamine, supplemented with 10% FBS, SCF (50 ng ml^{-1}), IL-3 (10 ng ml^{-1}) and IL-6 (10 ng ml^{-1}). To improve cell adhesion to the slides, various coating methods (Fibronectin, Poly-D-Lysine, Lipopolysaccharide and ibiTreat tissue culture-treated slides from Ibidi) were tested, and ibiTreat slides were selected, as they showed the best cell adhesion. After 24 h of cell culture, cells were stained with a cocktail of three SAFE antibodies (5 μg ml^{-1}, 10 minues at room temperature) and quenched with BHQ3-N-Tz (1 μM, 5 minutes at room temperature) for each cycle.

Imaging. Cells were imaged in live-cell imaging solution (Thermo Fisher Scientific, A14291DJ) at room temperature. Images were collected using a custom-made Olympus FV1000 confocal multi-photon system using a ×60 LUMFL N water immersion objective (NA = 1.1, Olympus America). Fluorescent channels were imaged sequentially with 405-nm, 473-nm, 559-nm and/or 635-nm lasers using a 405/473/559/635 dichroic to separate excitation light and dichroic beam splitters SDM473, SDM560 and SDM640 to separate emission light. Fluorophore signals were further separated using emission filters BA430-455, BA490-540, BA575-620 and BA655-755. Each fluorescence channel was imaged sequentially using distinct excitation and emission filter sets to ensure minimal bleed-through between channels. All lasers, beam splitters and emission filters were purchased from Olympus. For the final cycle of the imaging sequence, cells were co-incubated with calcein blue AM (Thermo Fisher Scientific, C1429; see also Supplementary Fig. 9).

ER-Hoxb8 differentiation model. *ER Hoxb8 cell culture.* ER-Hoxb8 cells were derived from the bone marrow of male ER-KO C57BL/6 CD45.1^{STEM} mice[68]. Detailed protocols for construction of the retroviral vector encoding ER-Hoxb8, virus production and transduction of bone marrow myeloid progenitor cells were described previously[43] and are available online: https://sykeslab.com/reagent-request. In brief, bone marrow mononuclear cells were isolated and expanded in medium containing SCF, IL-6 and IL-3 (10 ng ml^{-1}) for 48 h. Cells were placed in 12-well plates pre-coated with human fibronectin (Sigma-Aldrich, F-0895) and spin-infected with murine stem cell virus encoding ER-Hoxb8, as previously described. Infected cells were cultured in RPMI medium containing SCF (20 ng ml^{-1}) and β-estradiol (500 nM) for 2 days before addition of G418 for selection. The cells were passaged to new plates with fresh medium every 3–4 days, and non-adherent immortalized cells grew out in about 3 weeks. These cells were maintained in culture no more than 4 weeks (six-well culture plate) until needed for microwell imaging experiments.

ER-Hoxb8 longitudinal microwell imaging. ER-Hoxb8 cells were imaged longitudinally on days 0, 2, 4 and 6. On day 0, cells were stained with a cocktail of two SAFE-conjugated antibodies (anti-CD45 and anti-cKit) for 10 minutes at 4 °C. The antibodies were diluted to 5 μg ml^{-1} in cell culture media with β-estradiol as stated above. The stained cells were washed three times with the cell culture media with β-estradiol. After washing, live-cell imaging solution (Thermo Fisher Scientific, A14291DJ) containing 0.1 mM Trolox (Vector Laboratories, CB1000-2) was added to the cells for imaging. Images were acquired with a DeltaVision inverted fluorescence microscope, with the exposure time set to 100 ms to minimize phototoxicity to the living cells across multiple imaging sessions. Quenching was performed with BHQ3-N-Tz (**2**) diluted to 500 nM in cell culture media with β-estradiol and incubated with cells for 10 minutes at room temperature. After quenching, cells were washed with cell culture media without β-estradiol for three times and placed back in the incubator for further culture. On days 2, 4 and 6, the same procedure was conducted with two cycles of staining and quenching. The first cycle included staining with a cocktail of three SAFE-conjugated antibodies (anti-CD45(MB594), anti-cKit(anti-Rat-647) and anti-F4/80(AF488)); the second cycle included staining with a cocktail of the remaining three SAFE-conjugated antibodies (anti-Ly6C(MB594), anti-Ly6G(AF647) and anti-CD11b(MB488)). Each image captured a set of 12 microwells, and four imaging sites on the chip were captured in each profiling session (n = 48 wells total).

Neutrophil differentiation—flow cytometry control experiments. ER-Hoxb8 immortalized progenitors and SCF-dependent neutrophil progenitors were kept on ice for all steps if not stated otherwise. Cells were washed and resuspended in PBS and stained with Zombie Aqua fixable viability dye (BioLegend, 423101) to exclude dead cells. Cells were washed with PBS and incubated with FcBlock (clone

93, BioLegend) for 15 minutes at 4 °C, followed by staining with fluorescently conjugated antibodies for 25 minutes at 4 °C in staining buffer (0.5% BSA in PBS). The cells were washed with staining buffer and analyzed on a LSRII flow cytometer (BD). The following cell populations were identified based on cell marker expression: ER-Hoxb8 immortalized progenitors ($CD45^+CD11b^-cKit/CD117^+$) and neutrophils ($CD45^+CD11b^+cKit/CD117^-Ly6G^+$). Antibodies are reported in Supplementary Table 2.

Reporting summary. Further information on research design is available in the Nature Research Reporting Summary linked to this article.

Data availability

All data that support the observations and conclusions of the study are included in the manuscript and its Supplementary Information. Raw multi-channel and/or *z*-stack source data from time series images are available in TIF format at https://doi.org/10.5281/zenodo.6482316.

References

68. Mercier, F. E., Sykes, D. B. & Scadden, D. T. Single targeted exon mutation creates a true congenic mouse for competitive hematopoietic stem cell transplantation: the C57BL/6-CD45.1^{STEM} mouse. *Stem Cell Rep.* **6**, 985–992 (2016).

Acknowledgements

We are grateful to the Sykes Laboratory for preparing live bone marrow cells and to C. Carlson-O'Fallon for assistance with imaging data analysis. This work was supported, in part, by grants from the CSB development fund (J.C.T.C.), R01CA257623 (R.W.), UH3CA202637 (R.W.), R01CA206890 (R.W. and M.P.), P01CA069246 (R.W.), U01CA206997 (R.W.), P01CA240239 (M.P.) and R01CA229777 (R.W.). J.K. was supported by the Schmidt Science Fellows and K99CA256353.

Author contributions

Design: J.C.T.C., J.K. and R.W. Synthesis: M.W., H.M. and J.C.T.C. Experiments: J.K., J.O., E.B. and J.C.T.C. Data analysis: all authors. Writing: J.C.T.C., J.K., R.W. and all others.

Competing interests

The authors declare the following competing interests. J.C.T.C., R.W. and H.M. declare the filing of a patent (PCT/US2021/053439, pending; Bioorthogonal linkers and reactions), which was assigned to Massachusetts General Hospital. R.W. is a consultant to ModeRNA, Tarveda Therapeutics, Lumicell, Seer, Earli, Aikili Biosystems and Accure Health, consultancies that are unrelated to the subject matter of this work.

Additional information

Supplementary information The online version contains supplementary material available at https://doi.org/10.1038/s41587-022-01339-6.

Correspondence and requests for materials should be addressed to Ralph Weissleder or Jonathan C. T. Carlson.

Peer review information *Nature Biotechnology* thanks Christian Schürch and the other, anonymous, reviewer(s) for their contribution to the peer review of this work.

Reprints and permissions information is available at www.nature.com/reprints.

nature research

Corresponding author(s): Jonathan C.T. Carlson
Ralph Weissleder

Last updated by author(s): Apr 25, 2022

Reporting Summary

Nature Research wishes to improve the reproducibility of the work that we publish. This form provides structure for consistency and transparency in reporting. For further information on Nature Research policies, see our Editorial Policies and the Editorial Policy Checklist.

Statistics

For all statistical analyses, confirm that the following items are present in the figure legend, table legend, main text, or Methods section.

n/a	Confirmed
☐	☒ The exact sample size (*n*) for each experimental group/condition, given as a discrete number and unit of measurement
☐	☒ A statement on whether measurements were taken from distinct samples or whether the same sample was measured repeatedly
☒	☐ The statistical test(s) used AND whether they are one- or two-sided *Only common tests should be described solely by name; describe more complex techniques in the Methods section.*
☒	☐ A description of all covariates tested
☒	☐ A description of any assumptions or corrections, such as tests of normality and adjustment for multiple comparisons
☒	☐ A full description of the statistical parameters including central tendency (e.g. means) or other basic estimates (e.g. regression coefficient) AND variation (e.g. standard deviation) or associated estimates of uncertainty (e.g. confidence intervals)
☒	☐ For null hypothesis testing, the test statistic (e.g. *F*, *t*, *r*) with confidence intervals, effect sizes, degrees of freedom and *P* value noted *Give P values as exact values whenever suitable.*
☒	☐ For Bayesian analysis, information on the choice of priors and Markov chain Monte Carlo settings
☒	☐ For hierarchical and complex designs, identification of the appropriate level for tests and full reporting of outcomes
☒	☐ Estimates of effect sizes (e.g. Cohen's *d*, Pearson's *r*), indicating how they were calculated

Our web collection on statistics for biologists contains articles on many of the points above.

Software and code

Policy information about availability of computer code

Data collection	Microscopy data were collected with Metamorph (Olympus, version 7.8.6.0) and FV10 (Olympus, version 4.1.1.5). Flow cytometry data was collected in the integrated FACS Diva package (BD LSRII, Becton Dickinson). No open source or custom code was used.
Data analysis	FlowJo (version 10.8.0), GraphPad Prism (version 9), ImageJ (version 2.0.0), Numbers (Apple, version 10.0), and Microsoft Excel (version 16.53) were used for data analysis.

For manuscripts utilizing custom algorithms or software that are central to the research but not yet described in published literature, software must be made available to editors and reviewers. We strongly encourage code deposition in a community repository (e.g. GitHub). See the Nature Research guidelines for submitting code & software for further information.

Data

Policy information about availability of data

All manuscripts must include a data availability statement. This statement should provide the following information, where applicable:

- Accession codes, unique identifiers, or web links for publicly available datasets
- A list of figures that have associated raw data
- A description of any restrictions on data availability

All data that support the observations and conclusions of the study are included in the manuscript and its Supplementary Information. Raw multichannel and/or Z-stack source data from time series images are available in TIF format at https://doi.org/10.5281/zenodo.6482316 .

Field-specific reporting

Please select the one below that is the best fit for your research. If you are not sure, read the appropriate sections before making your selection.

☒ Life sciences ☐ Behavioural & social sciences ☐ Ecological, evolutionary & environmental sciences

For a reference copy of the document with all sections, see nature.com/documents/nr-reporting-summary-flat.pdf

Life sciences study design

All studies must disclose on these points even when the disclosure is negative.

Sample size	No sample size calculations were performed, as the results describe the capabilities of the (bio)chemical methodology across a diverse set of experimental contexts, rather than quantifying biological population-specific interventions/phenomena. Sample sizes for imaging-based biological analyses in adherent and/or microwell culture were thus chosen on the basis of pilot studies that established the expected density of cells under a given set of loading conditions and longitudinal proliferation. Additional experimental rationales are reported figure-by-figure as follows: Fig. 2D, kinetics: Hundreds of A431 cells are visible per individual field of view; the intensity profile methodology provides an unbiased method to quantify signal clearance kinetics. Fig. 3A/B, live-cell pilot experiments: Hundreds of A549 cells per field of view illustrate scission performance; given the striking visual dynaic range, no quantitative parameters are reported. Fig. 3C, murine PBMCs: Based on an estimated minimum loading density of 10 cells/well, 6 fields of view (72 wells) were imaged, with the final total of 737 cells comfortably exceeding an empiric threshold of 500 cells. At this scale, excellent correlation with flow cytometry was observed for both marker abundance (R^2 = 0.99) and cell viability. At the experimental sample size (SAFE 737 cells, FLOW 32,500 cells), post hoc power analyses (alpha 0.05) indicate a 99.3% power to detect a hypothetical two-fold increase in the abundance of dead cells (observed: 3.5% SAFE vs 3.8% FLOW). Figs. 4/5. No quantitative parameters are reported. Fig. 6, Hoxb8 neutrophil experiments: we again applied an empiric threshold target of ~500 cells at the start of the experiment (48 wells, ≥10 cells/well); proliferation of the cells over the course of the 6 day study increased this number to ≥500 cells per field of view (609 cells are present the image used to generate the ring plot in Fig 6B), sufficient to qualitatively observe the expected asynchronous timing of cellular differentiation [Wang, G. G. et al. Quantitative production of macrophages or neutrophils ex vivo using conditional Hoxb8. Nat Methods 3, 287-293 (2006)].
Data exclusions	No data were excluded from the experimental results or analyses.
Replication	The numbers of experimental replicates conducted are reported within the text and/or accompanying figure legends within the manuscript.
Randomization	The experiments reported characterize the chemical and biological performance of the SAFE platform. No biological samples were allocated into experimental groups for therapeutic or descriptive analyses.
Blinding	For the comparative analysis of cellular subset abundance by flow cytometry vs SAFE (Fig. 3D), the data were collected and analyzed independently by separate investigators (flow--JO; SAFE--JK) blinded to their counterpart's analysis. No aspects of the remaining experiments involved comparative analyses between cell populations, differentially treated biological samples, or primary tissue specimens where blinding would be relevant.

Reporting for specific materials, systems and methods

We require information from authors about some types of materials, experimental systems and methods used in many studies. Here, indicate whether each material, system or method listed is relevant to your study. If you are not sure if a list item applies to your research, read the appropriate section before selecting a response.

Materials & experimental systems

n/a	Involved in the study
☐	☒ Antibodies
☐	☒ Eukaryotic cell lines
☒	☐ Palaeontology and archaeology
☐	☒ Animals and other organisms
☒	☐ Human research participants
☒	☐ Clinical data
☒	☐ Dual use research of concern

Methods

n/a	Involved in the study
☒	☐ ChIP-seq
☐	☒ Flow cytometry
☒	☐ MRI-based neuroimaging

Antibodies

Antibodies used	The complete specifications of all antibodies used in the study are compiled in Supplementary Tables 1 & 2, accompanied by information on antibody dilution and staining concentration.

Validation	Cetuximab has previously been validated for specific EGFR targeting in the course of clinical development and validated for immunofluorescent applications (Haun, J. B., et al., Nat Nanotechnol 5, 660-665 (2010); Ko, J., et al., Angew Chem Int Ed Engl 59, 6839-6846 (2020)). Antibodies for other targets were selected from panels established/validated in prior published work (Ko, J., et al., Angew Chem Int Ed Engl 59, 6839-6846 (2020); Oh, J. et al., Clin Cancer Res clincanres.1252.2021 (2021)), and were specifically validated by their manufacturers for immunofluorescence, immunocytochemistry, and/or flow cytometry. Finally, all new antibody conjugates were validated against conventional immunofluorescence imaging (secondary antibody staining) on positive cell lines or mouse splenocytes before usage in SAFE imaging.

Eukaryotic cell lines

Policy information about cell lines

Cell line source(s)	A431 and A549 cells were obtained from the American Tissue Culture Collection (ATCC)
Authentication	New stocks of A549 (CCL-185) and A431 (CRL-1555) were obtained from ATCC immediately prior to the experiments as validated source material and used directly without further in house storage or re-validation.
Mycoplasma contamination	All cell lines tested negative for mycoplasma contamination.
Commonly misidentified lines (See ICLAC register)	No commonly misidentified lines were used.

Animals and other organisms

Policy information about studies involving animals; ARRIVE guidelines recommended for reporting animal research

Laboratory animals	Bone marrow and peripheral blood were harvested from C57BL/6J mice (female, age 8-12 weeks). Mouse liver imaging experiments were performed with hepatic tissue harvested from C57BL/6J MerTK-GFP mice (female, 12 weeks old) [Mohan et al., 2017, Proc Natl Acad Sci U S A, 114, E7776-E7785]. Housing conditions for the mice: Temperature is set to 68F- 73F Humidity is set to 30%-70% Light/dark cycle is 12 h light/12 h dark from 7 am to 7 pm light; 7 pm to 7 am dark
Wild animals	The study did not involve wild animals.
Field-collected samples	The study did not involve samples collected from the field.
Ethics oversight	Ethics oversight was provided by the Institutional Animal Care and Use Committee (IACUC) for Massachusetts General Hospital and Shriner's Hospital, approved under Animal Protocols 2013N000157 (murine tissue harvest and imaging) and 2017N000255 (murine bone marrow harvest and culture).

Note that full information on the approval of the study protocol must also be provided in the manuscript.

Flow Cytometry

Plots

Confirm that:

☒ The axis labels state the marker and fluorochrome used (e.g. CD4-FITC).

☒ The axis scales are clearly visible. Include numbers along axes only for bottom left plot of group (a 'group' is an analysis of identical markers).

☒ All plots are contour plots with outliers or pseudocolor plots.

☒ A numerical value for number of cells or percentage (with statistics) is provided.

Methodology

Sample preparation	As described in detail in the Online Methods, whole blood was collected from C57BL/6J mice by cardiac puncture and processed by density gradient centrifiugation (Lymphoprep, Stem Cell Technologies). Cells were washed after staining and strained through a 40 µm filter prior to analysis on the flow cytometer.
Instrument	Flow cytometer: Becton Dickinson LSRII.
Software	Data were collected on the BD LSRII with FACS Diva and analysed in FlowJo (version 10.8.0, BD)
Cell population abundance	Cell population abundance is depicted in Figure 3D; no cell-sorting or fractionation was performed.
Gating strategy	The gating strategy is supplied in detail in Supplementary Figure 6. Briefly, cells were gated by forward and side scatter as indicated, followed by exclusion of dead cells by from DAPI staining and confirmation of CD45 pan-positivity. The CD45

positive cells were then fractionated by expression of their respective lymphoid and myeloid marker subpopulations as indicated.

☒ Tick this box to confirm that a figure exemplifying the gating strategy is provided in the Supplementary Information.